Preprints of the 19th World Congress
The International Federation of Automatic Control
Cape Town, South Africa. August 24-29, 2014

LPV Torque Vectoring for an Electric Vehicle with Experimental Validation ⋆

Gerd Kaiser, Matthias Korte *
Qin Liu, Christian Hoffmann and Herbert Werner **

* *Department of EE-Architecture, Intedis GmbH, 97084 Wuerzburg, Germany* - gerd.kaiser@intedis.com
** *Institute of Control Systems, Hamburg University of Technology, 21073 Hamburg, Germany* - www.tuhh.de/rts

Abstract: In this paper, we propose a torque vectoring controller for an electric vehicle with two electric machines which drive the front wheels independently. The torque vectoring system includes a vehicle dynamics controller and a motor torque and wheel slip limiter. The vehicle dynamics controller is designed as a polytopic, linear parameter-varying (LPV) gain-scheduled controller. The LPV controller tracks the longitudinal velocity and the yaw rate of the vehicle. A torque and slip limiter (TSL) is developed to deal with physical saturation of the electric motors and wheel slip limitations which are related to the traction of the tires. The TSL deals with actuator limitations and prevents the wheel from spinning or blocking. Following the design, the controller is converted into fixed-point representation and is implemented on an automotive-qualified microcontroller. As part of the European project eFuture, test drives are performed to obtain experimental data. For comparison the automotive prototype is driven with both, equal torque and the designed torque vectoring controller. The differences between the two approaches are illustrated with experimental results for a double lane change maneuver.

Keywords: LPV; Torque Vectoring; Application; Vehicle Dynamics; Electric Vehicles

1. INTRODUCTION

In future fewer vehicles will be equipped with pure combustion engines. The electrification of the drive train in hybrid electric vehicles is likely to continue (see Emadi [2005]). E.g. in California, the market share of hybrid cars (McPhaul [2013]) rose to 7.2 % in 2013 and with the electric vehicle "Tesla Model S" ranging third in sales of "Luxury and Sports" class cars. Electric motors simplify the decentralization of the drive train, which results in vehicle configurations with individually driven (two or four) wheels. With a distributed propulsion system, new safety and efficiency requirements are arising with the distribution of the propulsion system. These requirements are addressed for example in the European project eFuture (www.eFuture-eu.org). An electric vehicle prototype is developed in this project and is shown in Fig. 1.
The torque vectoring approach allows electric vehicles to be more effectively controlled if the vehicle is equipped with two or four electric motors. Different torque vectoring strategies have been addressed in Pinto et al. [2010], Liu et al. [2011], Wang et al. [2011], Chu et al. [2010] and Kaiser et al. [2011]. Each approach has certain disadvantages, which are discussed in Kaiser et al. [2012] and also solved in Bartels et al. [2013]. The basic idea of torque vectoring is that driver requests (steering angle, brake and acceleration pedal position) are processed and distributed as torque commands to the wheels of the vehicle. Therefore, the longitudinal and lateral dynamics must be controlled.

⋆ This work was supported by the European Commission under Grant agreement no. 258133.

Fig. 1. Prototype of the European project eFuture

In addition to the vehicle dynamics the controller has to take into account the limited wheel forces (see Pacejka [2006]). Finally a torque vectoring controller should be tunable for a trade-off between longitudinal and lateral driver requests in case of saturation. In Kaiser et al. [2012] a torque-vectoring scheme was proposed that is based on a continuous-time LPV vehicle dynamics controller and a continuous-time torque and slip limiter. The present work is a follow-up of Kaiser et al. [2012] and discusses the implementation issues of realizing a torque vectoring controller in a test vehicle with an automotive-approved microcontroller.
This paper is organized as follows: Section 2 reviews basic

properties of linear parameter-varying control. Section 3 describes the vehicle model. Section 4 outlines the controller design with the LPV controller and the torque and slip limiter. Section 5 specifies the fixed-point conversion, which is necessary for microcontroller implementation. Measurement results from test drives are presented in section 6. Section 7 provides conclusions about the designed torque vectoring controller.

2. LPV CONTROL

A polytopic, linear parameter-varying (LPV) torque vectoring controller has been proposed in Kaiser et al. [2012] and is used here to control the nonlinear vehicle model. During the last 20 years, LPV control is increasingly used for applications in the field of aeronautics (e.g. Bates and Hagstroem [2009]) and roboter control (e.g. Hashemi et al. [2012]). In LPV control, well-known linear design strategies, like H_∞ design, are extended to nonlinear systems. The proposed controller is based on a constant quadratic Lyapunov function and guarantees stability and performance in the entire parameter space. Mixed-sensitivity shaping filters are introduced to calibrate the controller. For the design, the plant $G(\theta)$ is rewritten as LPV model (Apkarian et al. [1995])

$$\begin{aligned} x(k+1) &= A(\theta)x(k) + B_w(\theta)w(k) + B_u(\theta)u(k) \\ z(k) &= C_z(\theta)x(k) + D_{wz}(\theta)w(k) + D_{uz}(\theta)u(k) \\ y(k) &= C_y(\theta)x(k) + D_{wy}(\theta)w(k) + D_{uy}(\theta)u(k). \end{aligned} \quad (1)$$

The state vector x, the exogenous input w and the control input u are used to calculate the control output z and the measured output y. The parameter-dependent matrices $A(\theta), B(\theta), C(\theta)$ and $D(\theta)$ are functions of $\theta \in \mathbb{R}^p$, where

$$\theta(k) = f_\theta(\rho(k)) \quad (2)$$

is a vector of scheduling parameters and $f_\theta : \mathbb{R}^l \to \mathbb{R}^p$ an analytic mapping of measurable scheduling signals $\rho(k) \in \mathbb{R}^l$ onto the admissible scheduling parameter set

$$\mathcal{P} \subset \mathbb{R}^p : \theta \in \mathcal{P}, \forall k > 0, \quad (3)$$

which is assumed to be compact. An affine model (1) in θ is represented in a polytopic form with

$$\left[\begin{array}{c|c} A(\theta) & B(\theta) \\ \hline C(\theta) & D(\theta) \end{array}\right] = \sum_{i=1}^{p} \theta_i \left[\begin{array}{c|c} A_i & B_i \\ \hline C_i & D_i \end{array}\right]. \quad (4)$$

Vertices of the parameter space are represented by the $\bullet_i$ model matrices. The exogenous input w and the control input u is combined in the input matrix B as $[B_w, B_u]^T$. In addition to the feedback law, a feed-forward part is included, as in Liu et al. [2011] and Kaiser et al. [2012] which uses the steering angle δ as disturbance signal. The controller $K(\theta)$ has the form

$$\begin{aligned} x_c(k+1) &= A_c(\theta)x_c(k) + B_{ce}(\theta)e(k) + B_{cw}(\theta)w(k) \\ u(k) &= C_c(\theta)x_c(k) + D_{ce}(\theta)e(k) + D_{cw}(\theta)w(k). \end{aligned} \quad (5)$$

A controller is calculated for every vertex of the polytopic parameter set, with the shape defined in Fig. 3. An LPV controller that guarantees stability and performance in the whole parameter set is then obtained by interpolating among the individual vertex controllers; for more details see Apkarian et al. [1995].

3. VEHICLE MODEL

Several vehicle models have been proposed to describe the dynamics of an automotive vehicle. The model should be of complexity as low as possible for controller realization. For torque vectoring longitudinal, lateral and yaw dynamics are important. Also the constraints of the electric motors have to be considered. Fig. 2 shows the relevant quantities. Mathematically, the vehicle dynamics can be described by the nonlinear single track model

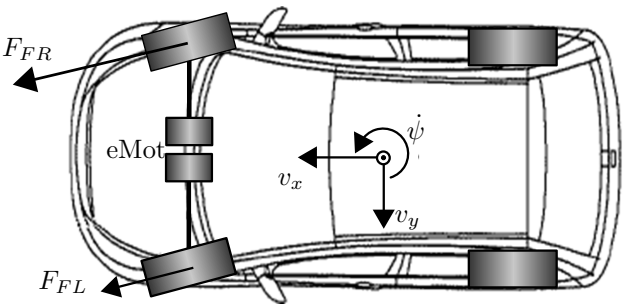

Fig. 2. Drive train architecture of eFuture with two electric machines

Table 1. Definition of the simulation model variables

sign	value	comment
l_f	1.240	distance front axle to center of gravity[m]
l_r	1.228	distance rear axle to center of gravity [m]
$C_{y,f}$	70,000	cornering stiffness of the front axle [N]
$C_{y,r}$	84,000	cornering stiffness of the rear axle [N]
w_f	1.445	front axle width [m]
M	1492	vehicle mass [kg]
I_z	1800	moment of inertia around vertical axis [kg m^2]

$$\dot{v}_\mathrm{x} = v_\mathrm{y}\dot{\psi} + \frac{1}{M}\left(F_\mathrm{FL} + F_\mathrm{FR}\right) \quad (6)$$

$$\begin{aligned} \dot{v}_\mathrm{y} = &-v_\mathrm{x}\dot{\psi} - \frac{C_{y,f} + C_{y,r}}{M v_\mathrm{x}} v_\mathrm{y} \\ &+ \frac{l_r C_{y,r} - l_f C_{y,f}}{M v_\mathrm{x}}\dot{\psi} + \frac{C_{y,f}}{M}\delta \end{aligned} \quad (7)$$

$$\begin{aligned} \ddot{\psi} = &\frac{l_r C_{y,r} - l_f C_{y,f}}{I_z v_\mathrm{x}} v_\mathrm{y} - \frac{l_f^2 C_{y,f} + l_r^2 C_{y,r}}{I_z v_\mathrm{x}}\dot{\psi} \\ &+ \frac{l_f C_{y,f}}{I_z}\delta + \frac{w_f}{2I_z}(F_\mathrm{FR} - F_\mathrm{FL}). \end{aligned} \quad (8)$$

Here v_x represents the longitudinal velocity, v_y the lateral velocity and $\dot{\psi}$ the yaw rate of the vehicle. The model inputs are the steering input δ and the longitudinal tire forces F_FL for the front left wheel and F_FR for the front right wheel. The physical parameters are defined in Table 1. The model is reasonably accurate for $v_\mathrm{x} > 3\frac{m}{s}$. However, numerical problems for (6 - 8) arise for low velocities and the model is even undefined for standstill and the physical representation is not correct for reverse driving. It is assumed that the vehicle tire slip λ and the tire slip angle α are small, i.e. $|\lambda| < 0.1$, $|\alpha| < 0.08$ rad. For discrete-time controller synthesis, the vehicle model must be in a discrete-time form. The Euler forward conversion (see Toth et al. [2010]) is used to convert the model into this form because certain properties of the LPV-plant model must be preserved for the synthesis. More sophisticated and accurate designs like the Euler backward or Tustin approximation (again Toth et al. [2010],Haugen [2005]) would violate the assumption of Apkarian et al. [1995]. In this approach, the matrices D_{uz} and D_{wy} must be

parameter-independent and $D_{uy} = 0$.
The representation as LPV model is not unique; here we choose the scheduling parameters as

$$\begin{aligned} \theta_1 &= \frac{1}{v_\mathrm{x}} & \theta_2 &= \dot{\psi} \\ x &= \left[v_\mathrm{x}, v_\mathrm{y}, \dot{\psi}\right]^T & u &= [F_\mathrm{FL}, F_\mathrm{FR}]^T \\ w &= \delta & y &= \left[v_\mathrm{x}, \dot{\psi}\right]^T, \end{aligned} \tag{9}$$

which results in a discrete-time model $G(\theta)$ as in (1) with the polytopic LPV form

$$\begin{aligned} A(\theta) =& I + T_s \left(A_0 + \theta_1 A_1 + \theta_2 A_2\right) \\ =& I + T_s \begin{bmatrix} 0 & \theta_2 & 0 \\ -\theta_2 & -\dfrac{C_{\mathrm{y,f}} + C_{\mathrm{y,r}}}{M}\theta_1 & \dfrac{C_{\mathrm{y,r}} l_\mathrm{r} - C_{\mathrm{y,f}} l_\mathrm{f}}{M}\theta_1 \\ 0 & \dfrac{C_{\mathrm{y,r}} l_\mathrm{r} - C_{\mathrm{y,f}} l_\mathrm{f}}{I_\mathrm{z}}\theta_1 & -\dfrac{C_{\mathrm{y,r}} l_\mathrm{r}^2 + C_{\mathrm{y,f}} l_f^2}{I_z}\theta_1 \end{bmatrix} \\ B_w =& T_s \begin{bmatrix} 0 \\ \dfrac{C_f}{M} \\ \dfrac{C_f l_{x,f}}{I_z} \end{bmatrix}, \quad B_u = T_s \begin{bmatrix} \dfrac{1}{M} & \dfrac{1}{M} \\ 0 & 0 \\ -\dfrac{w_f}{2I_z} & \dfrac{w_f}{2I_z} \end{bmatrix} \\ C_\mathrm{y} = C_\mathrm{z} =& \begin{bmatrix} 1 & 0 & 0 \\ 0 & 0 & 1 \end{bmatrix}, \quad D_\mathrm{wz} = D_\mathrm{uz} = D_\mathrm{wy} = D_\mathrm{uz} = \mathbf{0}. \end{aligned}$$

where, w is the exogenous input, u the controller input and T_s the sampling time.

4. CONTROLLER DESIGN

In order to realize the torque vectoring controller on a microcontroller, it is necessary to describe the controller in a discrete time representation. For the mixed sensitivity design of a gain-scheduled LPV controller filters are designed and heuristically tuned. The filters are parameter dependent in order to achieve improved tuning capabilities and better closed-loop performance. For example, the yaw rate error should not be considered for low velocities but is crucial for high vehicle velocities. A discrete-time, parameter-varying, sensitivity shaping filter $W_s(\theta)$, with sampling frequency 100 Hz, is heuristically tuned and set to

$$W_s(\theta) = \left[\begin{array}{c|c} A_s(\theta) & B_s \\ \hline C_s & D_s \end{array}\right] = \left[\begin{array}{cc|cc} -0.005 & 0 & 0.25 & 0 \\ 0 & -66.6667\theta_1 & 0 & 1 \\ \hline 0.2 & 0 & 0 & 0 \\ 0 & 0.6667 & 0 & 0 \end{array}\right].$$

The parameter dependent, discrete-time control sensitivity filter $W_k(\theta)$ is similar constructed and tuned to

$$W_k(\theta) = \left[\begin{array}{cc|cc} -500 & 0 & 8 & 0 \\ 0 & -498.48 - 55.08\theta_1 & 0 & 32 \\ \hline -14.0625 & 0 & 0.25 & 0 \\ 0 & -28.125 & 0 & 2 \end{array}\right].$$

After defining the shaping filters, the plant model from (9) must be augmented with the shaping filter form the generalized plant $G(\theta)$, as in (1). This step is straightforward is discussed e.g. in Skogestad and Postlethwaite [2005].
A discrete-time, polytopic linear parameter-varying controller is designed (see Apkarian et al. [1995] or Apkarian et al. [1996]). Two scheduling parameters are sufficient for the LPV-plant description, but using six vertices—instead of four—significantly improves the controller performance. The coordinates are defined in Fig. 3.

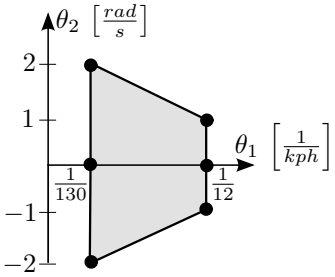

Fig. 3. Scheduling parameter space

4.1 Discrete-time torque and slip limiter

In Kaiser et al. [2012] a torque and slip limiter (TSL) is integrated into the torque vectoring function. Physical saturations of the electric motors and tire slip limitations degrade the performance of the designed LPV controller. An anti-windup scheme (see Turner and Postlethwaite [2004]) is used to preserve stability and suppress windup effects in case of motor saturation. The anti-windup approach is extended to limit the tire slip of the vehicle because spinning or blocking wheels deteriorate the performance, efficiency and safety. For realization, discrete-time calculation (as in Turner et al. [2003]) is used to find the suboptimal, static anti-windup gains. The LTI-concept from Turner et al. [2003] is applied to every vertex. Then the LTI anti-windup vertex compensators are linearly interpolated. A detailed explanation of the TSL scheme is given in Kaiser et al. [2012].

4.2 Controller structure

The controller structure is shown in Fig. 4. Reference signals are calculated with a nonlinear single track model. The concept of reference generation is described in Kaiser et al. [2011] and Poussot-Vassal [2008].
In the unsaturated case, the LPV controller receives the error signal e as an input. The disturbance $w = \delta$ is included to achieve feed forward control. The output of the controller u represents a request to the electric motors. In the implementation a geometric factor gF is included to convert the controller output $u = [F_x, M_z]^T$ to the electric motor torque requests $[T_\mathrm{FL}, T_\mathrm{FR}]^T = gF[F_x, M_z]^T$.
In the case of motor saturation $\Delta u \neq 0$ or excessive tire slip $|\lambda| > \lambda_{lim}$ the TSL is activated and changes the closed-loop behaviour. As shown in Fig. 4, the TSL output y_1 modifies the controller output u in order to limit the controller request. The TSL output y_2 is added to the control error e in order to suppress the wind-up of the LPV controller.

5. FIXED-POINT REPRESENTATION

The microcontroller, Freescale Bolero MPC5607B, is used in the eFuture project. The torque vectoring function is calculated with a sampling time of 0.01 s. In addition, five major functions must be calculated by the same microcontroller. The automotive software standard AUTOSAR (see Roebuck [2012]) has to be used - which creates some additional overhead for the base software calculation. So the final requirement for the execution time of torque vectoring is that the compiled software code must run within 1 ms on the microcontroller. To execute the generated code

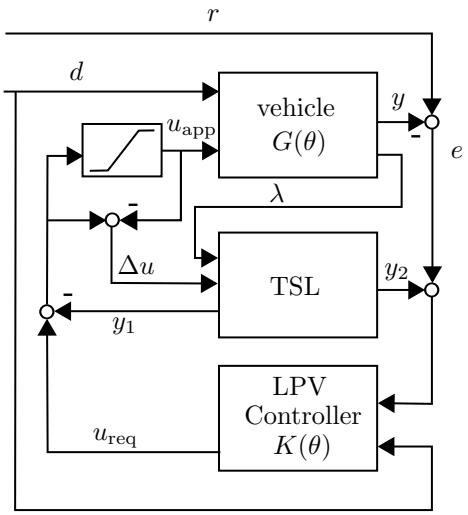

Fig. 4. Overall control structure

within this limit, the software must be converted to a fixed-point representation (see Granas and Dugundji [2003]). Drawbacks of the fixed-point representation are the risks of overflows and the possibility of an inaccurate representation. However, this process is required to reduce the online computation effort. It is useful to normalize the controller model at the beginning and the controller at the end. A suitable fixed-point conversion strategy with a state space controller is explained in Jerez et al. [2012].
For the Bolero microcontroller, it is necessary to limit also the bit size of every signal. The inputs to an accumulator can have a maximum of 32 bits. For efficient code execution, the multiplication and memory storage signals are limited to 16 bits. Calculations like square root or trigonometric functions must be replaced by suitable lookup tables. In the end, with all these modifications the microcontroller needs 0.7 ms to update torque vectoring.

6. MEASUREMENT RESULTS

As part of the eFuture project, several test drives are performed with the prototype. During every test about 430 signals have been logged; here the nine most important signals for torque vectoring will be discussed. In particular, the double lane change test (ISO 3888-2, also known as "elk-" or "moose-test") will be discussed because this test is well known and it dynamically effects the lateral dynamics of the vehicle.
However, with a human driver in the loop, it is difficult to compare the measurement results because the driver behaves differently in every test. To reduce this effect, the same driver always operates the vehicle for a given test.

6.1 Double lane change

The double lane change (DLC) is a closed-loop test, where a human driver operates the vehicle at its lateral tire force limits. The test is considered successful, if the driver is able to follow the track without touching a cone. The test starts with the driver heading into the cone setup, as shown in Fig. 5. The driver must perform subsequently a strong left turn, a strong right turn and again a strong

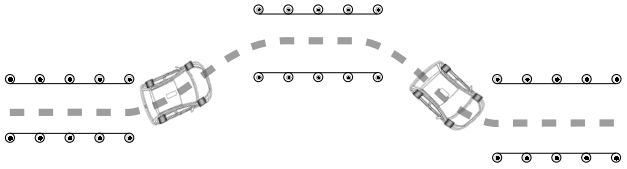

Fig. 5. Double lane change - cone setup

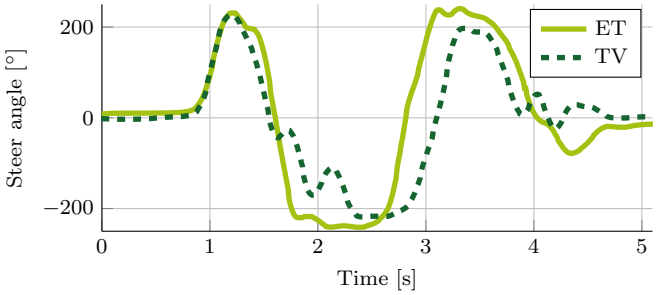

Fig. 6. Steering wheel angle

left turn. For the longitudinal requests, the neutral gear is engaged right before reaching the first set of cones. With the engaged neutral gear, the longitudinal drive request is set to zero, which simplifies the analysis of the lateral vehicle properties. Up to now, the driver is able to successfully perform the DLC-test with an equal torque (ET) distribution and a maximum initial velocity of 58 kph. With torque vectoring (TV) the same driver is able to succeed in the test with a maximum of 63 kph. In the following the DLC with ET and with TV are compared in order to see the different vehicle behaviour. The successful TV-test is compared with an ET-test. The same initial velocity is driven, but the driver is not able to successfully perform the test with ET.
In Fig. 6 the steering input of the driver is compared. At the beginning both steering commands are quite similar but for the right turn (1.8 - 2.6 s) the driver has to steer 20 degrees more and for the second left (3 - 3.6 s) turn even 40 degrees more. With equal torque the driver steers the second left turn earlier than with torque vectoring.

Fig. 7 shows the longitudinal velocity comparison of the vehicle with equal torque and with torque vectoring. Both vehicles start with nearly the same velocity of 63.5 kph and 64 kph. The vehicle with torque vectoring has a velocity of 52 kph after the last cone setup. The vehicle with equal torque has 46 kph at the end. Why this velocity difference occurs is not totally clear. Rajamani and Piyabongkarn [2013] showed that distributed longitudinal forces have no effect on the total lateral forces of the tires. This is also observed here in the lateral acceleration of the vehicle (which is not shown in this paper but is quite similar). However, the longitudinal tire forces influence the distribution of the lateral tire forces. So with the ET-configuration once the front tire forces and once the rear tire forces are closer to the maximum, lateral tire force which results in a higher difference of the side slip angles of the tyres. The higher wheel slip angle difference results in higher lateral tire powers and therefore a higher lateral energy loss of the vehicle, which slows down the ET-configuration stronger.

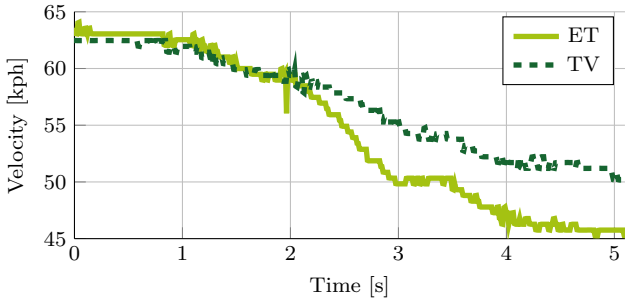

Fig. 7. Longitudinal velocity

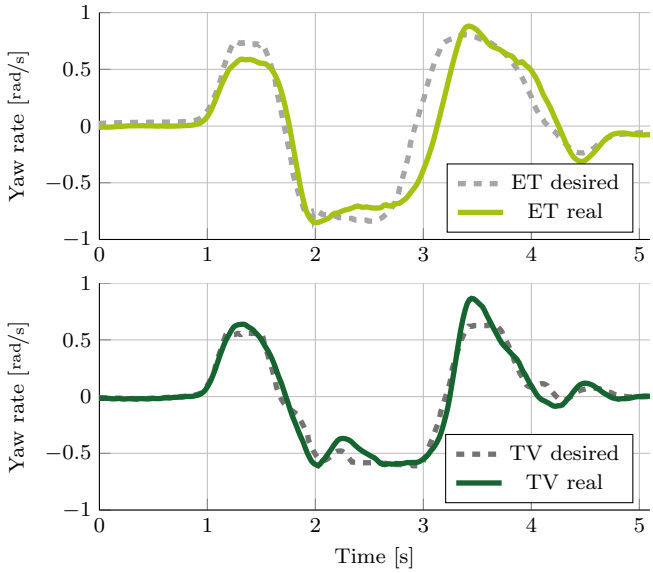

Fig. 8. Vehicle yaw rate

Fig. 8 shows two plots comparing the desired yaw rate and the measured yaw rate for both vehicle configurations. The maximum desired yaw rate with equal torque is 0.86 rad/s and therefore higher than the maximum desired yaw rate for torque vectoring with 0.61 rad/s. The higher maximum desired yaw rate is directly related to the higher steering effort of the ET-configuration. The most important difference is the faster response of the TV-configuration. This can be seen from the second left steer maneuver between 2.8 and 3.3 s, where the desired and real yaw rate for TV are much closer.
In Fig. 9 the torque for the ET configuration is 0 Nm all the time, which is related to the neutral gear request from the driver. For torque vectoring the torque of the left and right motor are in opposite directions. The TSL is necessary because the actuators are limited. For the DLC maneuver the physical slew rate limitation of the electric motors is the main drawback, which can be seen e.g. between 3.1 and 3.45 s. The slew rate limitation is responsible for the overshoots and the delay between desired and real yaw rate.

Fig. 10 does not show the longitudinal tire slip of the ET-configuration because the tire slip is zero all the time, where no torque is applied. For torque vectoring the tire slip of the front right wheel reaches the value of -0.28 at 2.5 s with a negative motor torque of -425 Nm. This slip value is not critical, but with a "softer" TSL

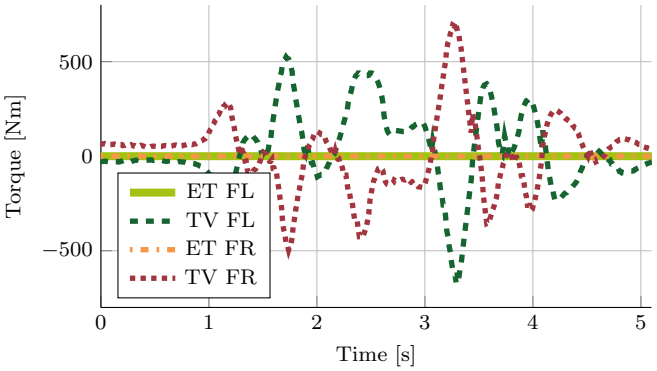

Fig. 9. Electric motor torque

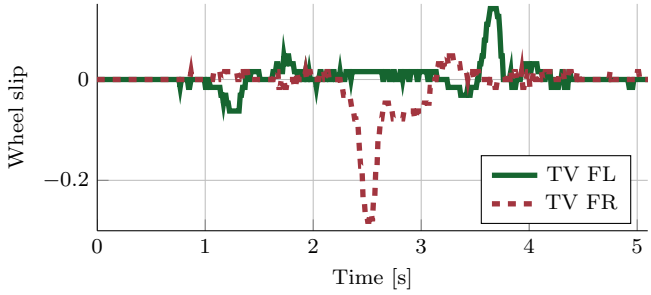

Fig. 10. Longitudinal tire slip

tuning the front right wheel even starts to block, which degrades the performance and safety of the vehicle. At time 1.75 s a stronger negative torque of -495 Nm does not have this negative wheel slip effect. Reviewing videos of the test drive shows that this problem is caused by the roll movement of the vehicle. Between 2 s and 3 s, the vehicle is in a strong right curve and the front right wheel nearly looses contact to the ground, so the vertical force acting onto this wheel is very low and the wheel can spin or block very easily. With a proper tuning of the TSL, this problem is solved.
Up to now the difference between equal torque and torque vectoring have been explained based on the measured outputs and inputs, but it is not completely clear why the driver is able to perform the DLC with torque vectoring and fails with equal torque. In fact, a major difference in the vehicle behaviour becomes evident when comparing the vehicle side slip angles β in Fig. 11 - where β is the angle between the direction the vehicle is pointing to and the direction the vehicle is moving to. During the test drive with torque vectoring the maximum side slip angle is limited to 0.13 rad, but with equal torque the side slip angle rises to 0.25 rad. With the "high" side slip angle of 0.25 rad (15 degree), the vehicle is difficult to maneuver and the vehicle behaviour is not stable anymore. A video comparing both tests can be found at: `http://www.tuhh.de/~rtsql/GK_IFAC2013.html`.

7. CONCLUSION

This paper presents the design, a real-time implementation and experimental validation of a LPV torque-vectoring controller on a test vehicle. During the eFuture project, several vehicle tests have been performed. In this paper, the results of the double lane change are shown because this is a standard test and it shows the influence of torque

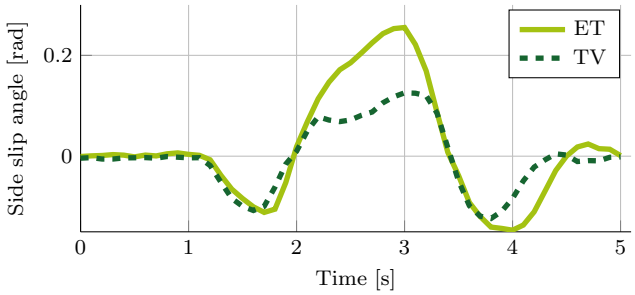

Fig. 11. Vehicle side slip angle

vectoring on dynamic lateral vehicle movement very well. Positive effects of torque vectoring, like reduced steering effort, better yaw rate tracking and reduced side slip angle are shown. The vehicle behaviour with equal torque and with torque vectoring is different. In general, if the controller is properly tuned, the vehicle behaviour is improved. So all requirements of the project are fulfilled.
However, during this work several new challenges appeared. For example the roll motion of the vehicle has an impact on the maximum longitudinal and lateral tire forces, which makes tuning of the TSL difficult. Also torque vectoring uses the longitudinal tire force difference to maneuver the vehicle, but different longitudinal front wheel forces have an impact to the steering wheel. So torque vectoring creates a feedback to the driver which influences the steering behaviour and leads to an ocilating steering behaviour of the driver, which was not appreciated by the test drivers. In future these two effects will be investigated to further improve the driver feeling while operating a vehicle with torque vectoring.

REFERENCES

Pierre Apkarian, Pascal Gahinet, and Greg Becker. Self-scheduled Hinf Control of Linear Parameter-Varying Systems: a Design Example. *Automatica*, 31(9):1251–1261, 1995.

Pierre Apkarian, Greg Becker, Pascal Gahinet, and Hiro Kajiwara. *LMI Techniques in Control Engineering from Theory to Practice*. IEEE, 1996.

Marcus Bartels, Qin Liu, Gerd Kaiser, and Herbert Werner. LPV Torque Vectoring for an Electric Vehicle. In *American Control Conference*, pages 2156–2161, 2013.

Declan Bates and Martin Hagstroem. *Nonlinear Analysis and Synthesis Techniques for Aircraft Control*. Springer, Berlin Heidelberg, 2009.

Liang Chu, Mingfa Xu, Yongsheng Zhang, Yang Ou, and Yanru Shi. Vehicle Dynamics Control Based on Optimal Sliding Mode Control Theory. In *Conference on Computer, Mechatronics, Control and Electronic Engineering*, pages 486–491, Changchun, China, 2010.

Ali Emadi. *Handbook of Automotive Power Electronics and Motor Drivers*. CRC Press, 2005.

Andrzej Granas and James Dugundji. *Fixed Point Theory*. Springer, New York, 2003.

Seyed Mahdi Hashemi, Hossam Seddik Abbas, and Herbert Werner. Low-complexity linear parameter-varying modeling and control of a robotic manipulator. *Control Engineering Practice*, 20(3):248 – 257, 2012.

Finn Haugen. *Discrete-time signals and systems*. TechTeach, 2005.

Juan L. Jerez, George A. Constantinides, and Eric C. Kerrigan. Towards a Fixed Point QP Solver for Predictive Control. In *IEEE 51st Annual Conference on Decision and Control (CDC)*, pages 675–680, Maui, Hawaii, USA, 2012.

Gerd Kaiser, Frederic Holzmann, Benoit Chretien, Matthias Korte, and Herbert Werner. Torque Vectoring with a feedback and feed forward controller. In *Intelligent Vehicles Symposium*, pages 448–453, Baden-Baden, Germany, 2011.

Gerd Kaiser, Qin Liu, Christian Hoffmann, Matthias Korte, and Herbert Werner. Torque vectoring for an electric vehicle using an LPV drive controller and a torque and slip limiter. In *Conference on Decision and Control*, pages 5016–5021, Maui, Hawaii, USA, 2012.

Qin Liu, Gerd Kaiser, S. Boonto, Herbert Werner, Frederic Holzmann, Benoit Chretien, and Matthias Korte. Two-Degree-of-Freedom LPV Control for a through-the-Road Hybrid Electric Vehicle via Torque Vectoring. In *Conference on Decision and Control*, pages 1274 – 1279, Orlando, USA, 2011.

Kim McPhaul. *California Auto Outlook*, volume 9. California New Car Dealers Association, 2013.

Hans B. Pacejka. *Tyre and Vehicle Dynamics*. Elsevier, Oxford, 2006.

Lorenzo Pinto, Simon Aldworth, Martin Watkinson, Paul Jeary, and Maria Franco-Jorge. Advanced Yaw Motion Control of a Hybrid Vehicle using Twin Rear Electric Motors. In *Advanced Vehicle Control Conference (AVEC)*, pages 640–645, Loughborough, UK, 2010.

Charles Poussot-Vassal. *Robust multivariable linear parameter varying automotive global chassis control*. PhD thesis, Grenoble INP, 2008.

Rajesh. Rajamani and Damrongrit Piyabongkarn. New paradigms for the integration of yaw stability and rollover prevention functions in vehicle stability control. *Intelligent Transportation Systems, IEEE Transactions on*, 14(1):249–261, March 2013.

Kevin Roebuck. *AUTOSAR - AUTomotive Open System ARchitecture*. Emereo Publishing, 2012.

Sigurd Skogestad and Ian Postlethwaite. *Multivariable feedback control analysis and design*. Wiley-Interscience, 2 edition, 2005.

Roland. Toth, Peter S. C. Heuberger, and Paul M. J. van den Hof. Discretisation of linear parameter-varying state-space representations. *Control Theory Applications, IET*, 4(10):2082–2096, October 2010.

Matthew C. Turner and Ian Postlethwaite. A new perspective on static and low order anti-windup synthesis. *International Journal of Control*, 77(1):27–44, 2004.

Matthew C. Turner, Guido Herrmann, and Ian and Postlethwaite. Discrete-Time Anti-Windup: Part 1 - Stability and Performance. In *European Control Conference; ECC'03*, pages 80–85, Cambridge, UK, 2003.

Junnian Wang, Qingnian Wang, Chuanxue Song, Liang Chu, and Yingying Wang. Coordinated control of differential drive assisted steering system with vehicle stability enhancement system. In *Intelligent Vehicles Symposium (IV)*, pages 1148 –1155, Baden-Baden, Germany, 2011.